RSC Advances

PAPER

Check for updates

Cite this: *RSC Adv.*, 2022, **12**, 16772

A curcumin-based AIEE-active fluorescent probe for Cu^{2+} detection in aqueous solution†

Yang Lin, Ao Yu, Jinjing Wang, Derui Kong, Hongtao Liu,* Jianwei Li* and Chunman Jia*

Received 23rd April 2022
Accepted 30th May 2022

DOI: 10.1039/d2ra02595g

rsc.li/rsc-advances

Curcuminoids have been extensively investigated as metal ion probes, but the intrinsic aggregation-caused-quenching (ACQ) characteristic of curcumin would hinder their applications in aqueous solution. Fortunately, tetraphenylethylene (TPE) could endow the compounds with aggregation-induced emission (AIE)/aggregation-induced enhanced emission (AIEE) characteristics to eliminate the ACQ effect. According to this strategy, a series of TPE-modified curcumin derivatives **L1–4** were prepared and studied for their AIEE properties. Among the four TPE-curcumin analogues, only **L1** particles have been successfully used as an on-off fluorescence probe for detecting Cu^{2+} in aqueous solution. The fluorescence titration experiment determined its detection limit of 1.49×10^{-7} mol L^{-1}, and the binding ratio between **L1** and Cu^{2+} was estimated as 2 : 1, which was in agreement with the results of high resolution mass spectrum and Job's plot. In addition, the binding constant was evaluated as 6.77×10^{2} M^{-1} using a Benesi–Hildebrand plot. Finally, the obtained **L1**-based indicator paper showed significant fluorescence response to Cu^{2+} aqueous solution. This TPE-modified strategy improves the detection capability of curcumin probe in aqueous solution and provides a feasible way to obtain other probes with ACQ characteristics.

1 Introduction

Curcumin is a natural yellow pigment extracted from the dried rhizomes of turmeric, which has low cytotoxicity, high photostability, and large two-photon absorption cross section.[1] In recent years, some curcumin-like fluorescent probes have been prepared and used to detect soluble/insoluble amyloids,[2] intracranial reactive oxygen species,[3] cysteine,[4] cancer cells,[5] and so on. From the point of view of its structure, the α,β-unsaturated β-diketone moiety can coordinate with a variety of metal ions, and many curcumin–metal complexes have been adopted as therapeutic agents for cancer, arthritis, osteoporosis, neurological disorders, and others.[6] Therefore, curcumin has great potential as a metal ion probe. However, curcumin and its derivatives usually have poor water-solubility, and their photophysical properties are strongly influenced by solvent, water, and pH. For example, Ali *et al.* have revealed that water could quench the fluorescence of curcumin in acetone by forming non-fluorescent stable charge-transfer complexes.[7] Bong has reported that the increased concentration of water could decrease the fluorescence intensity of curcumin.[8] This may be attributed to the non-radiative decay resulting from π–π stacking in the aggregation state, which is often named the aggregation-caused quenching (ACQ) effect. In order to overcome this problem, Patil and coworkers prepared *J*-aggregated curcumin nanoparticles (CURNPs) by the reprecipitation method with the surfactant Tween-80 in aqueous solution, which could retain the fluorescence properties of the curcumin monomer due to the separated molecule and no aggregation by lateral π-bonds.[9] The CURNPs had an on-off fluorescence response for Cu^{2+} with a low detection limit. However, it is essential to resolve this problem intrinsically by optimizing the molecular structure.

Encouragingly, two novel photoluminescence (PL) processes, namely aggregation-induced emission (AIE) and aggregation-induced emission enhancement (AIEE), can alleviate the ACQ effect by modifying the molecular structure with AIE/AIEEgens.[10–12] The AIE/AIEE molecules usually have negligible/low-intensity fluorescence in good solvents but enhanced emission intensity in nano aggregated states. To date, there have been prepared many varieties of AIE/AIEE-based nanoparticles as fluorescent probes for biological imaging and chemical sensing in water or high water content environments.[13–16] These probes exhibit bright emission with high fluorescent quantum yields in aggregated states. As one of the typical AIEgens, the highly twisted tetraphenylethylene (TPE) will limit the non-radiative energy transfer by hampering the intermolecular π–π stacking in aggregated states. Therefore, the TPE-based

Hainan Provincial Key Lab of Fine Chem, School of Chemical Engineering and Technology, Hainan University, Haikou 570228, China. E-mail: jiachunman@hainanu.edu.cn; jianwei.li@utu.fi; liuhongtao@hainanu.edu.cn

† Electronic supplementary information (ESI) available. CCDC 2167438. For ESI and crystallographic data in CIF or other electronic format see https://doi.org/10.1039/d2ra02595g

This article is licensed under a Creative Commons Attribution-NonCommercial 3.0 Unported Licence.

(cc) BY-NC

© 2022 The Author(s). Published by the Royal Society of Chemistry

fluorescent probes have outstanding fluorescent response and recognition capability in aqueous solutions.[17–19]

Inspired by the above, herein we tried to synthesize AIE/AIEE-active curcumin derivatives by introducing the TPE-moiety. As shown in Scheme 1, four TPE-curcumin analogues are prepared by using different substituents on the curcumin moieties, namely TPE-C-OMe (**L1**), TPE-C-H (**L2**), TPE-C-Cl (**L3**), and TPE-C-N(Me)$_2$ (**L4**). According to the experimental results, **L1–3** all possess notable AIEE properties in the THF/water mixtures with different water fractions (f_ws), but only **L1** has the potential to be a fluorescent probe for Cu^{2+} detection. In addition, **L1** particles were prepared by using a simple reprecipitation method without any surfactant and displayed high Cu^{2+} fluorescent response with good anti-interference capability, low detection limit, and fast response time. Finally, we adopted **L1** to prepare a fluorescent indicator paper and verified its application potential for the rapid and effective detection of Cu^{2+} in water.

2 Experimental

2.1 Materials and instruments

All reagents were purchased from commercial sources and used without further purification unless otherwise stated. All experimental water used was deionized water.

^{1}H and ^{13}C NMR spectra were recorded on a Bruker AV 400 NMR spectrometer (Bruker, Switzerland) by using deuterated chloroform as solvent and tetramethylsilane as internal standard. High resolution mass spectrometry (HRMS) were obtained on a LCMS-IT-TOF high resolution mass spectrometer (Shimadzu, Japan). Fluorescence spectra were recorded on a HORIBA Fluorolog-3 high-sensitivity fluorescence spectrometer (HORIBA, Japan). Single crystal X-ray diffraction data were performed on a Bruker APEX-II CCD diffractometer. During the data collection process, the crystals was kept at 150 K.

2.2 Synthesises of the compounds

2.2.1 Synthesis of compound 1. A DMSO solution of acetylacetone (1.2 g, 3.07 mmol), 1-iodo-4-(1,2,2-triphenylethenyl) benzene[20] (1.4 g, 12.28 mmol), K_2CO_3 (1.7 g, 12.28 mmol), cuprous iodide (58.5 mg, 0.31 mmol), and levoprotiline (70.7 mg, 0.61 mmol) was stirred at 90 °C for 6 h under a nitrogen atmosphere. After cooling to room temperature, the solution was poured into 1.0 M hydrochloric acid. Then, the mixture was extracted with ethyl acetate, and the organic layer was washed with brine and dried with anhydrous sodium sulfate before concentration under vacuum. Finally, the resulting crude product was purified by silica gel column chromatography using petroleum ether/ethyl acetate (10/1, v/v) as eluent to give 0.7 g white solid. Yield: 67.8%. ^{1}H NMR (400 MHz, chloroform-*d*) δ 7.16–6.99 (m, 17H), 6.90 (d, J = 8.0 Hz, 2H), 1.86 (s, 6H). ^{13}C NMR (100 MHz, chloroform-*d*) δ 190.96, 143.79, 143.46, 143.34, 143.26, 141.62, 140.67, 135.08, 131.77, 131.46, 131.41, 131.35, 130.48, 127.87, 127.82, 127.60, 126.70, 126.63, 115.06, 24.17. HRMS (ESI), m/z: $[M + Na]^+$ = 453.1817 (calcd for $C_{31}H_{27}O_2^+$, 453.1825).

2.2.2 Synthesis of compound L1. Compound **1** (100.2 mg, 0.23 mmol) and boronic anhydride (9.7 mg, 0.14 mmol) were dissolved in 3 mL of ethyl acetate and stirred at 40 °C for 30 min. Then the mixture was added with *p*-anisaldehyde (56 μL, 0.46 mmol) and tributyl borate (125 μL, 0.46 mmol). After stirring for another 30 min, *n*-butylamine (23 μL, 0.23 mmol) dissolved in 3 mL ethyl acetate was added dropwise to the mixture over 20 min. The mixture was continued to stir for 4 h at 40 °C, then 6 mL 1 N hydrochloric acid was added to the mixture, and the mixture was heated and stirred at 60 °C for 1 h. After cooling to room temperature, the mixture was separated to organic layer and aqueous phase, and the aqueous phase was extracted with dichloromethane for three times. The combined organic layers were washed with 30 mL water, and then dried over anhydrous Na_2SO_4. After solvent evaporation, the crude product was purified by silica gel column chromatography using petroleum

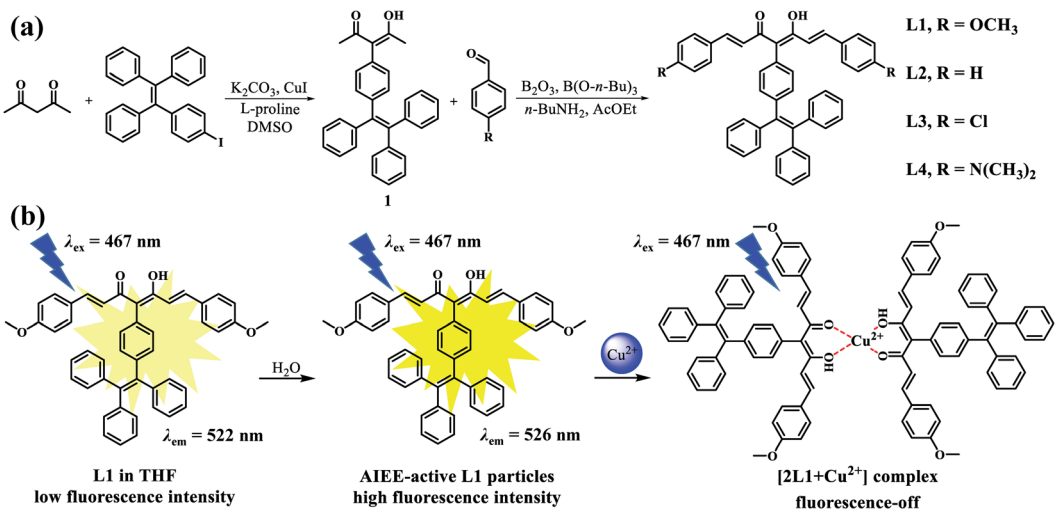

Scheme 1 (a) Synthetic routes of L1–4; (b) schematic representation of L1 for Cu^{2+} detection.

© 2022 The Author(s). Published by the Royal Society of Chemistry

ether/dichloromethane (10/1, v/v) as eluent to give 89.8 mg yellow solid. Yield: 58.8%. ^{1}H NMR (400 MHz, chloroform-*d*) δ 7.63 (d, J = 15.7 Hz, 2H), 7.31 (d, J = 8.6 Hz, 4H), 7.21–7.03 (m, 19H), 6.90 (d, J = 8.6 Hz, 4H), 6.37 (d, J = 15.6 Hz, 2H), 3.86 (s, 6H). ^{13}C NMR (100 MHz, chloroform-*d*) δ 182.48, 161.34, 143.98, 143.66, 143.55, 143.53, 141.46, 140.72, 140.44, 133.73, 131.89, 131.62, 131.61, 131.44, 131.41, 129.95, 128.34, 127.88, 127.85, 127.76, 126.77, 126.76, 126.63, 120.29, 114.38, 55.55. HRMS (ESI), *m*/*z*: $[M - H]^-$ = 665.2680 (calcd for $C_{47}H_{37}O_4^-$, 665.2697).

2.2.3 Synthesis of compound L2. **L2** was synthesized by using the same procedure as **L1** to give 30.3 mg yellow-green solid. Yield: 21.5%. ^{1}H NMR (400 MHz, chloroform-*d*) δ 7.67 (d, J = 15.7 Hz, 2H), 7.37 (s, 10H), 7.24–7.01 (m, 19H), 6.51 (d, J = 15.7 Hz, 2H). ^{13}C NMR (100 MHz, chloroform-*d*) δ 182.49, 143.93, 143.79, 143.62, 143.50, 141.56, 140.93, 140.62, 135.47, 133.30, 131.81, 131.73, 131.62, 131.44, 131.41, 130.16, 128.93, 128.30, 127.90, 127.87, 127.78, 126.79, 126.69, 122.49, 116.42. HRMS (ESI), *m*/*z*: $[M + H]^+$ = 607.2631 (calcd for $C_{45}H_{35}O_2^+$, 607.2632).

2.2.4 Synthesis of compound L3. **L3** was synthesized by using the same procedure as **L1** to give 69.7 mg yellow solid. Yield: 45.1%. ^{1}H NMR (400 MHz, chloroform-*d*) δ 7.60 (d, J = 15.7 Hz, 2H), 7.34 (d, J = 8.5 Hz, 4H), 7.26 (d, J = 8.7 Hz, 4H), 7.20–7.00 (m, 19H), 6.45 (d, J = 15.7 Hz, 2H). ^{13}C NMR (100 MHz, chloroform-*d*) δ 182.25, 143.93, 143.55, 143.38, 141.69, 140.49, 139.61, 136.04, 133.90, 132.97, 131.75, 131.63, 131.41, 131.34, 129.42, 129.20, 127.91, 127.74, 126.88, 126.84, 126.65, 122.82, 116.55. HRMS (ESI), *m*/*z*: $[M - H]^-$ = 673.1706 (calcd for $C_{45}H_{31}Cl_2O_2^-$, 673.1707).

2.2.5 Synthesis of compound L4. **L4** was synthesized by using the same procedure as **L1** to give 55.2 mg red solid. Yield: 34.5%. ^{1}H NMR (400 MHz, chloroform-*d*) δ 7.69 (d, J = 15.5 Hz, 2H), 7.35 (d, J = 8.9 Hz, 4H), 7.31–7.10 (m, 19H), 6.74 (d, J = 8.7 Hz, 4H), 6.37 (d, J = 15.5 Hz, 2H), 3.12 (s, 12H). ^{13}C NMR (100 MHz, chloroform-*d*) δ 182.38, 151.64, 144.04, 143.76, 143.74, 143.02, 141.24, 140.96, 134.53, 132.03, 131.62, 131.49, 131.44, 130.02, 127.86, 127.81, 127.78, 126.67, 126.60, 117.77, 115.24, 111.96, 40.35. HRMS (ESI), *m*/*z*: $[M + H]^+$ = 693.3476 (calcd for $C_{49}H_{45}N_2O_2^+$, 693.3476).

2.3 Preparation of stock solution

L1–4 were dissolved in THF to prepare a stock solution with a concentration of 1.0 mmol L^{-1}, respectively. Various metal ion and anion compounds were dissolved in deionized water to prepare a stock solution with a concentration of 10.0 mmol L^{-1} respectively, including KCl, NaCl, $MgSO_4$, $MnSO_4$, $ZnCl_2$, $CaCl_2$, $FeCl_2$, $FeCl_3\cdot 6H_2O$, $CoSO_4$, $CuCl_2\cdot 2H_2O$, $Pb(CH_3COO)_2\cdot 2H_2O$, $AgNO_3$, $Al(NO_3)_3\cdot 9H_2O$, $Ni(CH_3COO)_2$, $Pb(CH_3COO)_2\cdot 2H_2O$, NaF, Na_2CO_3, Na_2S, Na_2SO_3, $NaHSO_3$, NaCl, Na_2SO_4, $NaNO_3$, $NaNO_2$, and NaBr.

2.4 Determination of the binding constant

The binding constant (K_B) was evaluated using modified Benesi–Hildebrand equation given below.[9]

$$\frac{1}{I - I_0} = \frac{1}{(I_{max} - I_0)} + \frac{1}{K_B(I_{max} - I_0)} \frac{1}{[Cu^{2+}]^n}$$

where I_{max} is the maximum fluorescence intensity of **L1** in presence of Cu^{2+}, and I_0 and I in absence and in the presence of Cu^{2+} ion solution respectively. $[Cu^{2+}]$ represents the concentration of Cu^{2+}, and "*n*" is the number of Cu^{2+} bound per **[2L1+Cu^{2+}]** complex. For Cu^{2+}, "*n*" is taken 0.5. The double-reciprocal plot of $1/(I - I_0)$ against $1/[Cu^{2+}]^{0.5}$ shown in Fig. S23.†

2.5 Determination of the detection limit

Based on the fluorescence titration experiment, the detection limit (DL) was determined by calculation.[21] Under constant conditions, the fluorescence intensity of 10 groups of fluorescent probe **L1** (1.00×10^{-5} mol L^{-1}) without the addition of Cu^{2+} at a wavelength of 525 nm was tested as a blank experiment and the standard deviation (SD) was calculated. Then, using the results of fluorescence titration experiment, the fluorescence intensity of probe **L1** after adding different concentrations of Cu^{2+} was plotted as the vertical coordinate and the concentration of Cu^{2+} was plotted as the horizontal coordinate, and the linear equation $y = kx + b$ was plotted by taking the point with better linearity, and finally, according to the formula: DL = 3*SD*/*k*, from which the DL of fluorescent probe **L1** for Cu^{2+} could be calculated.

2.6 Parameters of fluorescence test

All samples were tested after dripping the stock solution into the solvent for one minute. The slit width of **L2** and **L3** was 1.2/1.2 nm when measured both fluorescence spectra in different water/THF solutions (Fig. 3), and the slit width of other tests was 2.5/2.5 nm. All fluorescence intensities are expressed by dividing the original data by 10 000. The recognition capability (Fig. 4b) and anti-interference capability (Fig. 5) of **L1** were tested for four times, and the standard deviation was calculated according to four sets of experiments.

3 Results and discussion

3.1 Synthesis and structural characterization

As shown as in Fig. 1a, the intermediate **1** was synthesized by the CuI-catalyzed coupling reaction of 1-iodo-4-(1,2,2-triphenylethenyl)benzene and acetylacetone, and then the Adol reaction took place between intermediate **1** and benzaldehyde analogues with different *para*-substituents to obtain **L1–4**. All compounds were characterized by ^{1}H NMR, ^{13}C NMR, and HRMS. Detailed syntheses and characterizations are presented in Scheme 1a and Fig. S1–S16 in the ESI.† Furthermore, the single crystal of **L1** was successfully obtained by slow evaporation in the mixed solvent system (dichloromethane/methanol). According to the results of single crystal X-ray diffraction, the **L1** crystal is triclinic crystal system with $P\bar{1}$ space group (Table S1, CCDC 2167438).† Compared with the curcumin analogue without TPE moiety,[22] **L1** has a large torsion angle of 75.81° between the curcumin skeleton and the TPE moiety (Fig. 1a and b). As shown as in Fig. 1c, there is no effective π–π stacking in the extended-crystal structure of **L1**, which may be attributed to the twist molecular structure of TPE, and two phenyls of adjacent **L1**

© 2022 The Author(s). Published by the Royal Society of Chemistry

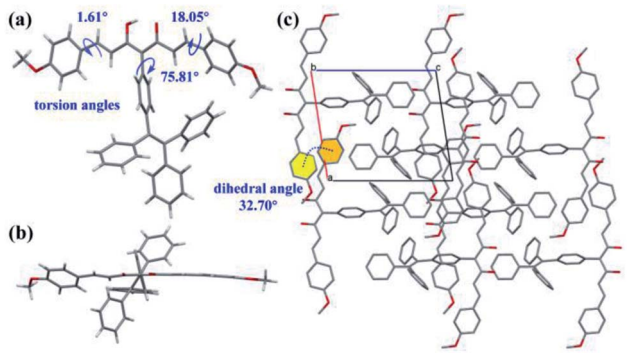

Fig. 1 The single crystal X-ray crystallography of L1: (a) top and (b) side views of single molecule; (c) the extended-crystal structure viewed from *b*-axis (the hydrogen atoms are hided for clarity). The hydrogen atoms are marked in white, carbon atoms in gray, and oxygen atoms in red.

molecules possess a dihedral angle of 32.70°. In addition, two adjacent parallel **L1** molecules in *b*-axis direction exhibit large stacking distances of 12.0 Å and 12.9 Å which are measured according to phenyls of curcumin skeleton (Fig. S17b and c).† As a result, the introduction of TPE in **L1** hinders the π–π stacking of phenyl in curcumin, which is beneficial to eliminate the ACQ effect.

3.2 Photophysical properties

The UV-vis absorption and fluorescence spectra of **L1–4** were measured in THF, and the detail optical data are shown in Table 1. As shown in Fig. 2a, **L1–4** have respective three inherent absorption bands. According to the literature, TPE has strong absorption in the range of 200–400 nm,[23] and curcumin has a max absorption peak of 390 nm in THF.[24] The introduction of TPE has red-shifted the absorption peak of curcumin from 390 to 413 nm (**L2**), which may be attributed to the electron-donating capability and the large conjugated structure of TPE. Furthermore, the substituents of methyl, chlorine, and dimethylamino also can make the same absorption peak red-shift, including 428 nm (**L1**), 430 nm (**L3**), and 487 nm (**L4**). However, the fluorescence spectra of **L1–4** in THF peaked at 522, 536, 548, and 562 nm, respectively. At the same time, the curcumin derivatives also showed large Stokes shift (Table 1), especially the shift values of **L2** and **L3** reached 123 and 118 nm, respectively, which could be attributed to their twist curcumin skeletons with greater photoinduced geometric changes.[25,26]

Table 1 Optical data of L1–4

Probe	λ_{abs} (nm)	λ_{ex} (nm)	λ_{em} (nm)	Stokes shift (nm)
L1	247, 327, 428	467	522	94
L2	244, 314, 413	419	536	123
L3	243, 318, 430	419	548	118
L4	245, 300, 487	467	562	75

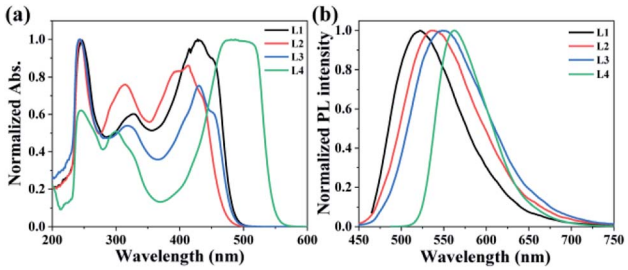

Fig. 2 Normalized (a) UV-vis absorption and (b) fluorescence spectra of L1–4 in THF.

3.3 AIEE properties

L1–4 have good solubilities in dichloromethane and THF but are insoluble in methanol and water. Since TPE is the classical AIEE-group, the AIEE properties of **L1–4** were investigated by testing their fluorescence spectra in THF/water mixtures with different f_ws. As shown as in Fig. 3a, the fluorescence intensity of **L1** is intensified with the f_w and reaches a maximum value with a red-shifted maximum emission peak (≈12 nm) at a f_w of 70%. This suggests that the aggregates of **L1** was formed in the solution with the increased f_w, which suppress the non-radiation energy loss. Thereafter, the higher f_w (≥80%) maybe induce worse molecular stacking which reduce the emission intensity due to the decreased AIEE effect. On the contrary, **L2** and **L3** (Fig. 3c and d) both have a decreased fluorescence intensity by increasing the f_w from 0% to 60%, which is attributed to the contribution of increased solvent polarity to twisted intramolecular charge transfer (TICT).[27] When the f_w increased from 60% to 99.99%, their emission intensity shows a sharp increase due to the AIEE effect. However, **L4** exhibits the bathochromic-shifted emission peak and the decreased fluorescence intensity with the gradual addition of water aside from $f_w \geq 80\%$. The stronger electron-donating capability of dimethylamine may increase the intramolecular charge transfer (ICT) which leading to the occurrence of fluorescence quenching.

3.4 Selectivity study

It has been reported that curcumin derivatives usually have good coordination capability with Cu^{2+}.[28] In the experimental process, only **L1** has rapid fluorescence response to Cu^{2+} in **L1–4**. The fluorescence intensity of **L1** in different THF/water mixtures was tested before and after adding one equivalent of Cu^{2+}. According to the experimental results shown in Fig. S18,† the **L1** solution ($V_{water}/V_{THF} = 4/1$) with higher fluorescence intensity is highly sensitive to Cu^{2+}, therefore the solution system ($f_w = 80\%$) was adopted in the following experiments. At the same time, the average aggregate size of **L1** was determined to 342 nm by dynamic light scattering (DLS) experiment as shown in Fig. S19.† Moreover, **L1** has a longer fluorescence lifetime (0.136 ns) in the THF/water solution ($f_w = 80\%$) than that (0.034 ns) in pristine THF, and the addition of Cu^{2+} significantly decrease the fluorescence lifetime to 0.030 ns. This

© 2022 The Author(s). Published by the Royal Society of Chemistry

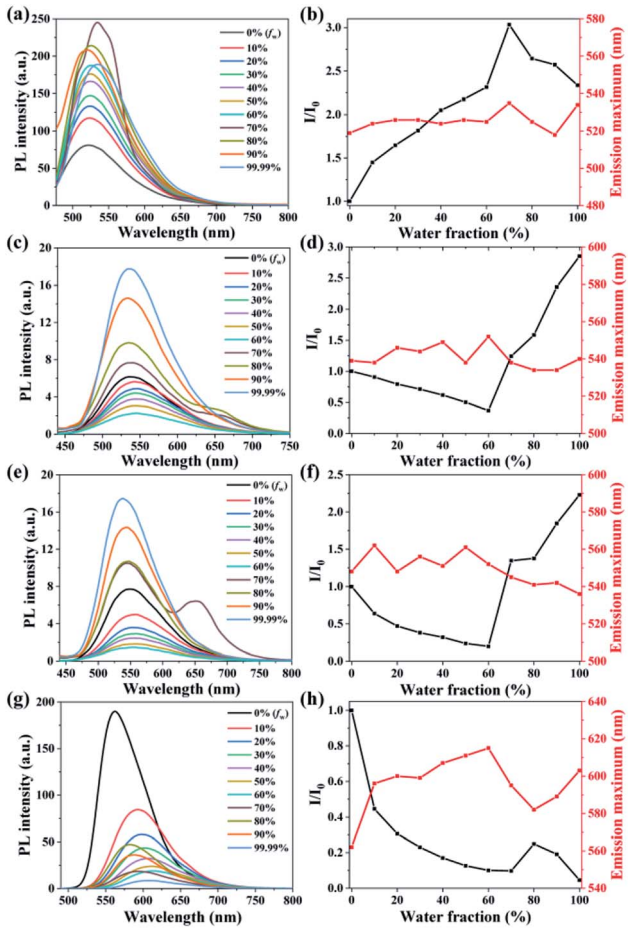

Fig. 3 Fluorescence spectra of (a) **L1**, (c) **L2**, (e) **L3**, and (g) **L4** in THF/water mixtures with different f_ws. Plots of relative fluorescent intensity (I/I_0) and fluorescence emission peaks of (b) **L1**, (d) **L2**, (f) **L3**, and (h) **L4** *versus* water fraction. I_0 is the fluorescence intensity of compound **L** in pristine THF solution (1×10^{-5} mol L^{-1}). The excitation wavelength (λ_{ex}) of **L1**, **L2**, **L3**, and **L4** is 467, 419, 419, and 467 nm, respectively.

illustrates that the formation of particles is favourable to enlarge the fluorescence lifetime of **L1**.

In order to determine the recognition capability of **L1** for various ions, the aqueous fluorescence spectra of **L1** were measured in the presence of one equivalent of different metal ions, including Na^+, K^+, Mg^{2+}, Ca^{2+}, Al^{3+}, Pb^{2+}, Mn^{2+}, Fe^{2+}, Fe^{3+}, Co^{2+}, Ni^{2+}, Cu^{2+}, Ag^+, and Zn^{2+}. As seen from Fig. 4, when adding one equivalent of metal cation into the **L1** aqueous solution (1×10^{-5} mol L^{-1}), a fluorescence quenching phenomenon with a quenching efficiency of 99% is only observed after the addition of Cu^{2+}, and other metal cations cause a slight decreased emission intensity but Al^{3+} marginally intensify the emission intensity about 14%. The electron-donating capability of methoxy enhances the binding ability of β-dicarbonyl in **L1** with metal ions through the conjugated effect, and the paramagnetic Cu^{2+} with underfilling 3d orbit combined with **L1** makes the energy or electron of fluorophore transfer, which leading to quenched fluorescence.[29] However, the substituents H and Cl have no effect on the combination between β-dicarbonyl and Cu^{2+}, and **L4** has no obvious phenomenon in the reaction with

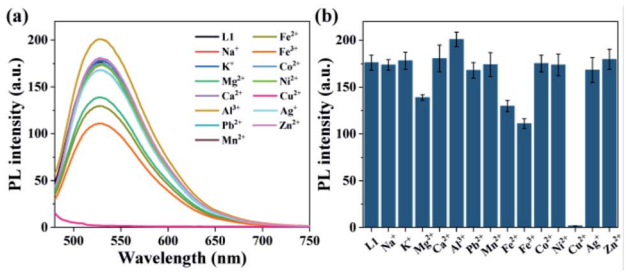

Fig. 4 (a) Fluorescence spectra and (b) fluorescence intensity changes of **L1** in the solution (1×10^{-5} mol L^{-1}, $V_{water}/V_{THF} = 4/1$) in the presence of one equivalent of different metal ions. The λ_{ex} is 467 nm.

Cu^{2+} due to its low fluorescence intensity in aqueous solution. Therefore, only **L1** possesses both AIEE feature and good selectivity for Cu^{2+} and can be used as a Cu^{2+} fluorescent probe in aqueous solution.

3.5 Anti-interference studies

The anti-interference capability of probe **L1** was tested by the competition experiments, which were carried out by adding one equivalent of Cu^{2+} into the **L1** solutions with ten equivalents of different competing ions. The used ions included metal cations (Cu^{2+}, Na^+, K^+, Mg^{2+}, Ca^{2+}, Al^{3+}, Pb^{2+}, Mn^{2+}, Fe^{2+}, Fe^{3+}, Co^{2+}, Ni^{2+}, Ag^+, Zn^{2+}) and anions (Br^-, Cl^-, F^-, S^{2-}, HCO_3^-, HSO_3^-, NO_3^-, NO_2^-, SO_3^{2-}, SO_4^{2-}, AcO^-). As shown in Fig. 5, the **L1** solutions with different competing ions all exhibit significant fluorescences which are quenched after the addition of Cu^{2+}. These results also demonstrate that **L1**-probe has excellent selectivity and specificity to Cu^{2+}. Especially, compared with the existing curcumin-based Cu^{2+} fluorescent probe,[9,22] **L1** also shows outstanding anti-interference capability to S^{2-}.

3.6 Influence of pH on probe L1

Curcumin is usually stable in acidity and unstable in neutrality and alkalinity,[30] it could degrade to produce vanillin, acetone, feruloylmethane, and ferulic acid in alkaline medium by hydrolytic splitting.[29] Therefore, it is essential to examine the detection capability of **L1** in response to Cu^{2+} at different pH.

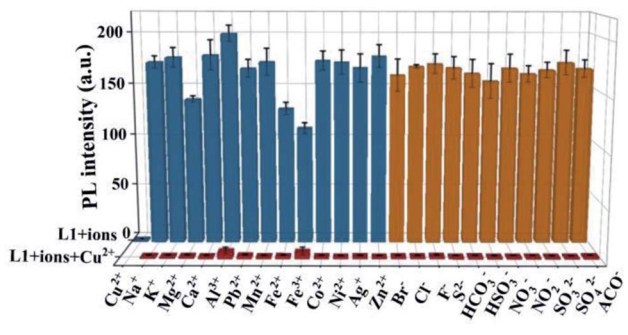

Fig. 5 Fluorescence intensity changes of **L1** in the presence of Cu^{2+} along with other cations and anions in the solution ($V_{water}/V_{THF} = 4/1$). The concentration of **L1** is 1×10^{-5} mol L^{-1}. The concentration of cation and anion are 1×10^{-4} mol L^{-1}, respectively. The λ_{ex} is 467 nm.

© 2022 The Author(s). Published by the Royal Society of Chemistry

The solutions ($V_{water}/V_{THF} = 4/1$) with pH values in the range of 2–13 were prepared by slowly adding a small amount of 1 M hydrochloric acid or sodium hydroxide solution with the detection of a pH meter. As shown in Fig. S20,† the fluorescence intensity of probe **L1** remains stable at pH 2–10 and gradually decreases at pH 11–13. The decreased emission intensity could be attributed to the degraded molecular structure of **L1**. Then, the fluorescence intensity of **L1** solution was quenched by adding Cu^{2+} at pH 5–11. As a result, the optimum pH-range is 5–10 for the application of probe **L1**.

3.7 Fluorescence titration experiment

The fluorescence titration experiment was carried out to determine the quantitative relationship between probe **L1** and Cu^{2+}. As shown in Fig. 6a, the fluorescence emission peak at 525 nm decreases continuously with the gradual addition of Cu^{2+}, and the fluorescence has been completely quenched after adding a half equivalent of Cu^{2+}. Therefore, the binding ratio between probe **L1** and Cu^{2+} can be determined as 2 : 1, which is in agreement with the result of the high resolution mass spectrum (Fig. S16†) and Job's plot (Fig. S22†). The mass spectrum peak of 1395.4503 ($[M - H]^+$, m/z) is belong to the complex [**2L1+Cu^{2+}**] (calculated for $C_{94}H_{75}CuO_8^+$, m/z: 1395.4786), and the peak of Job's plot is at 0.66. According to the Benesi–Hildebrand equation, the binding constant was calculated as 6.77×10^2 M^{-1} (Fig. S23†). In addition, the DL was calculated based on the fluorescence titration experiment (Fig. S24†) by using the IUPAC method. Ten sets of blank experiments were performed in the absence of Cu^{2+}, and the fluorescence emission intensity at 525 nm was adopted to calculate the SD to be 0.086. Based on the equation DL = 3SD/k, k is the slope of the calibration curve, **L1** has a DL of 1.49×10^{-7} mol L^{-1} for the detection of Cu^{2+}, which is decently low in comparison with other values of related works (Table S2†).

3.8 Cu^{2+} indicator paper

In order to explore the practical application potential of **L1**, a filter paper was soaked in THF solution containing **L1** (1 mM) for 5 s and dried in air to obtain a simple Cu^{2+} fluorescent indicator paper (Fig. 7a). Under the UV light of 365 nm, the indicator paper has no significant change after moistening with water (Fig. 7b), and the Cu^{2+} aqueous can effectively quench its fluorescence (Fig. 7c), for example, the word "HN" written with 0.01 mM Cu^{2+} aqueous solution on the indicator paper shows quenched fluorescence. Furthermore, the fluorescence responses of indicator paper to different concentration of Cu^{2+} aqueous solution were also investigated, and the fluorescence photographs and their fluorescence intensities are shown in Fig. 7d–g and S25,† respectively. After soaking in 0.01 mM Cu^{2+} aqueous solution for 10 s, the fluorescence intensity of obtained indicator paper has a sharp decline by 79.2% in comparison to that soaking in water. And the fluorescence intensities of indicator papers soaked in 0.1 mM and 1 mM Cu^{2+} aqueous solution maintain 14.4% and 10.9% of initial values, respectively. Additionally, the average color of indicator papers was also simulated, and the relative RGB values are shown in Fig. 7.

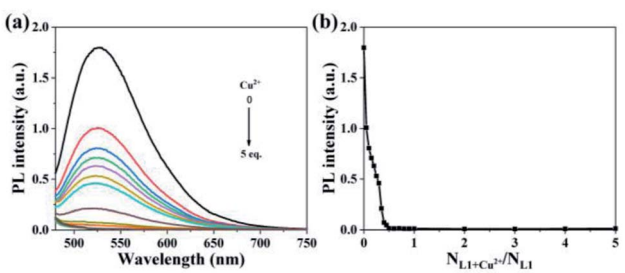

Fig. 6 (a) Fluorescence spectra and (b) fluorescence intensity plot at 525 nm of **L1** (1.00×10^{-5} mol L^{-1}) in the solution ($V_{water}/V_{THF} = 4/1$) with the continuous addition of Cu^{2+} (0–5 eq.).

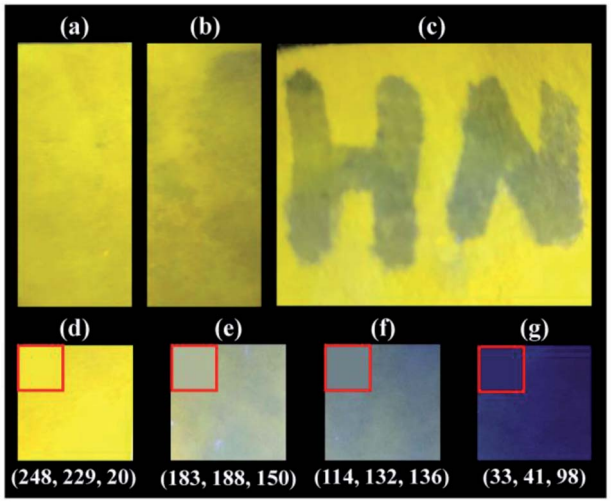

Fig. 7 Photographs under the UV light of 365 nm. **L1** fluorescent indicator paper: (a) pristine, (b) moistened with water, and (c) the word "HN" written with 0.01 mM Cu^{2+} aqueous solution on the indicator paper; dried **L1** fluorescent indicator papers after soaking in Cu^{2+} aqueous solutions with different concentrations for 10 s: (d) Cu^{2+}-free, (e) 0.01 mM, (f) 0.1 mM, and (g) 1 mM. The simulated average color is shown in the red box of respective picture, and the RGB information is shown in bracket.

4 Conclusions

In summary, a series of TPE-modified curcuminoids named **L1–4** have been designed and synthesized to improve the detection capability of curcumin-based fluorescent probe in aqueous solution. According to experimental results, different substituents on the curcumin moiety have different effects on the AIEE properties and Cu^{2+} recognition capability, and only methoxy-substituted **L1** has met both requirements simultaneously. The on-off fluorescent probe based on the **L1** particles possesses high selectivity, good anti-interference capability and rapid fluorescence recognition for Cu^{2+} detection, and its detection limit is as low as 149 nM. At the same time, a simple Cu^{2+} fluorescent indicator paper was prepared with **L1** and displayed effective and rapid detection for Cu^{2+} aqueous solution. This work demonstrates that the introduction of TPE is an effective

© 2022 The Author(s). Published by the Royal Society of Chemistry

strategy to enhance the fluorescent intensity and maintain the recognition capability of probe in aqueous solution, and it is necessary to optimize the molecular structure reasonably for achieving the optimal performance of probe.

Author contributions

Yang Lin: conceptualization, investigation, methodology, data curation, formal analysis, and writing – original draft. Ao Yu: investigation, methodology. Jinjing Wang: investigation, methodology. Derui Kong: investigation, data curation. Hongtao Liu: conceptualization, formal analysis, validation, and writing – review & editing. Jianwei Li: conceptualization, resources, funding acquisition, supervision, and writing – review & editing. Chunman Jia: conceptualization, resources, funding acquisition, supervision, project administration, and writing – review & editing. All authors contributed to discussions about the results and the manuscript.

Conflicts of interest

There are no conflicts to declare.

Acknowledgements

We are grateful for the financial support from the National Natural Science Foundation of China (22161017, 22161016) and the Start-up Research Foundation of Hainan University (KYQD(ZR)1852, KYQD(ZR)22034).

References

1 G. Xu, D. Wei, J. Wang, B. Jiang, M. Wang, X. Xue, S. Zhou, B. Wu and M. Jiang, *Dyes Pigm.*, 2014, **101**, 312–317.
2 C. Ran, X. Xu, S. B. Raymond, B. J. Ferrara, K. Neal, B. J. Bacskai, Z. Medarova and A. Moore, *J. Am. Chem. Soc.*, 2009, **131**, 15257–15261.
3 J. Yang, X. Zhang, P. Yuan, J. Yang, Y. Xu, J. Grutzendler, Y. Shao, A. Moore and C. Ran, *Proc. Natl. Acad. Sci. U. S. A.*, 2017, **114**, 12384–12389.
4 L. Pang, Y. Zhou, W. Gao, J. Zhang, H. Song, X. Wang, Y. Wang and X. Peng, *Ind. Eng. Chem. Res.*, 2017, **56**, 7650–7655.
5 Z. Pi, J. Wang, B. Jiang, G. Cheng and S. Zhou, *Mater. Sci. Eng., C*, 2015, **46**, 565–571.
6 S. Prasad, D. DuBourdieu, A. Srivastava, P. Kumar and R. Lall, *Int. J. Mol. Sci.*, 2021, **22**, 7094.
7 F. Jasim and F. Ali, *Microchem. J.*, 1992, **46**, 209–214.
8 P. H. Bong, *Bull. Korean Chem. Soc.*, 2000, **21**, 81–86.
9 D. P. Bhopate, P. G. Mahajan, K. M. Garadkar, G. B. Kolekar and S. R. Patil, *New J. Chem.*, 2015, **39**, 7086–7096.
10 J. Mei, N. L. Leung, R. T. Kwok, J. W. Lam and B. Z. Tang, *Chem. Rev.*, 2015, **115**, 11718–11940.
11 B.-K. An, J. Gierschner and S. Y. Park, *Acc. Chem. Res.*, 2012, **45**, 544–554.
12 H. Li, H. Kim, J. Han, V. N. Nguyen, X. Peng and J. Yoon, *Aggregate*, 2021, **2**, e51.
13 H. Wan, Q. Xu, P. Gu, H. Li, D. Chen, N. Li, J. He and J. Lu, *J. Hazard. Mater.*, 2021, **403**, 123656.
14 L. Biesen and T. J. J. Müller, *Aggregate*, 2021, **2**, e105.
15 Q. Lai, S. Si, T. Qin, B. Li, H. Wu, B. Liu, H. Xu and C. Zhao, *Sens. Actuators, B*, 2020, **307**, 127640.
16 Z. Luo, T. Lv, K. Zhu, Y. Li, L. Wang, J. J. Gooding, G. Liu and B. Liu, *Angew. Chem., Int. Ed.*, 2020, **59**, 3131–3136.
17 Y. Chen, W. Zhang, Y. Cai, R. T. K. Kwok, Y. Hu, J. W. Y. Lam, X. Gu, Z. He, Z. Zhao, X. Zheng, B. Chen, C. Gui and B. Z. Tang, *Chem. Sci.*, 2017, **8**, 2047–2055.
18 H.-F. Xie, C.-J. Yu, Y.-L. Huang, H. Xu, Q.-L. Zhang, X.-H. Sun, X. Feng and C. Redshaw, *Mater. Chem. Front.*, 2020, **4**, 1500–1506.
19 H. Wan, S. Zhou, P. Gu, F. Zhou, D. Lyu, Q. Xu, A. Wang, H. Shi, Q. Xu and J. Lu, *Poly. Chem.*, 2020, **11**, 1033–1042.
20 C. Y. K. Chan, J. W. Y. Lam, C. Deng, X. Chen, K. S. Wong and B. Z. Tang, *Macromolecules*, 2015, **48**, 1038–1047.
21 Y. Qian, L. Cao, C. Jia, P. O. Boamah, Q. Yang, C. Liu, Y. Huang and Q. Zhang, *RSC Adv.*, 2015, **5**, 77965–77972.
22 G. Xu, J. Wang, G. Si, M. Wang, X. Xue, B. Wu and S. Zhou, *Sens. Actuators, B*, 2016, **230**, 684–689.
23 L. Ding, L. Lin, C. Liu, H. Li, A. Qin, Y. Liu, L. Song, H. Zhang, B. Z. Tang and Y. Zhao, *New J. Chem.*, 2011, **35**, 1781–1786.
24 M. F. Raduly, V. Raditoiu, A. Raditoiu, L. E. Wagner and A. G. Liliana, *Rev. Chim.*, 2018, **69**, 1327–1331.
25 X. Liu, Z. Xu and J. M. Cole, *J. Phys. Chem. C*, 2013, **117**, 16584–16595.
26 V. A. Stepanova, A. Guerrero, C. Schull, J. Christensen, C. Trudeau, J. Cook, K. Wolmutt, J. Blochwitz, A. Ismail, J. K. West, A. M. Wheaton, I. A. Guzei, B. Yao and A. Kubatova, *ACS Omega*, 2022, **7**, 7257–7277.
27 J. Qi, C. Sun, A. Zebibula, H. Zhang, R. T. K. Kwok, X. Zhao, W. Xi, J. W. Y. Lam, J. Qian and B. Z. Tang, *Adv. Mater.*, 2018, **30**, 1706856.
28 T. Naghdi, S. Faham, T. Mahmoudi, N. Pourreza, R. Ghavami and H. Golmohammadi, *ACS Sens.*, 2020, **5**, 3770–3805.
29 G. Tamil Selvan, C. Varadaraju, R. Tamil Selvan, I. Enoch and P. Mosae Selvakumar, *ACS Omega*, 2018, **3**, 7985–7992.
30 Y.-J. Wang, M.-H. Pan, A.-L. Cheng, L.-I. Lin, Y.-S. Ho, C.-Y. Hsieh and J.-K. Lin, *J. Pharm. Biomed. Anal.*, 1997, **15**, 1867–1876.

© 2022 The Author(s). Published by the Royal Society of Chemistry